

Research Article

Mechanical and Microstructural Investigation on AZ91B Mg Alloys with Tool Tilt Variation by Friction Stir Welding

S. Yaknesh ¹, Mohammed Tharwan ², Rajasekaran Saminathan ², N. Rajamurugu ¹,
K. B. Prakash ³, Ankit ⁴, Manoj Kumar Pasupathi ⁵, Atul Sarojwal ⁶,
and Dawit Tafesse Gebreyohannes ⁷

¹Department of Aeronautical Engineering, Bharath Institute of Higher Education and Research, Chennai 600073, Tamil Nadu, India

²Department of Mechanical Engineering, College of Engineering, Jazan University, Jazan, Saudi Arabia

³Department of Mechanical Engineering, Bannari Amman Institute of Technology, Sathyamangalam, Erode 638401, Tamil Nadu, India

⁴Department of Mechanical Engineering, Government Engineering College, Jhalawar 326023, Rajasthan, India

⁵Department of Mechanical Engineering, KPR Institute of Engineering and Technology, Coimbatore 641407, Tamil Nadu, India

⁶Department of Electrical Engineering, FET, MJP Rohilkhand University, Bareilly 243006, UP, India

⁷Department of Mechanical Engineering, Faculty of Manufacturing, Institute of Technology, Hawassa University, Hawassa, Ethiopia

Correspondence should be addressed to Dawit Tafesse Gebreyohannes; dawitt@hu.edu.et

Received 1 August 2022; Revised 27 September 2022; Accepted 19 November 2022; Published 5 December 2022

Academic Editor: Guosong Wu

Copyright © 2022 S. Yaknesh et al. This is an open access article distributed under the Creative Commons Attribution License, which permits unrestricted use, distribution, and reproduction in any medium, provided the original work is properly cited.

By modifying the angle of tilt of 2 distinct tool pin shapes, both tapered with and without threaded structures, TPT tool pin with threads and TPNT tool pin with no threads, the mechanical behaviour and microstructural attributes were examined for the joints of AZ91B alloy formed by friction stir welding. Spindle torque and unique forces operating laterally and axially (referred to as Y-force and X-force, respectively) were created at the junction of the tool and plate, which were monitored and assessed in order to know the influence of degrees of tilt. When the tool's angle of tilt advances, torque and forces of the spindle also show an increasing trend that is important to friction stir welding. The spindle torque and Y-force produced by the TPT tool are higher than those of the TPNT tool, whereas the X-force associated with the TPT tool is less. Discrepancies in forces grow along the concurrent increase in the angle of tilt for the TPNT as well as TPT tools, exhibiting opposite behaviour. The onion ring-type structure was visualized in the threaded tool pin structure TPT due to the high flow of plasticized metal compared to TPNT tool joints, for which the onion ring shape is not visible. With the TPT tool, the joint made at a 0° angle of tilt had a peak tensile strength of 232 MPa.

1. Introduction

Alloys of magnesium (Mg) fall into the group that belongs to low dense, metallic characteristics, engineering materials and exhibit a variety of extensive and appealing properties such as exceptional electromagnetic shielding features, distinguished thermal conductivity, high degree of recyclability, greater specific strength, easily cast-able, and larger specific stiffness [1–3]. The presence of these qualities has enhanced the use of Mg alloys in a range of manufacturing

sectors, especially aerospace, marine, automotive, railroads, and electronics. On the other hand, Mg alloys have a limited range of uses because they are hard to shape at low room temperatures. This is because they have a densely packed hexagonal structure [4, 5].

Welding is the most important method for manufacturing in a variety of production industries and its applications. As well, identifying suitable welding processes for Mg alloys will be extremely beneficial in compensating for these alloys' lower formidability and extending their

applicability as engineering materials in a variety of sectors [6, 7]. As a result, it is critical to establish a suitable procedure for welding Mg alloys, particularly those in the AZ series, as they are generally used in a variety of production industries [8, 9].

Because friction stir welding (FSW), a high eminence, very effective, and environmentally friendly solid-state welding technique, is the best method to weld Mg alloys, FSW quickly avoids widespread solidification-related difficulties (such as constituent loss, grain roughening, and surface alteration) [10–12]. Moreover, because FSW is capable of combining Mg alloys without melting them, it can reasonably avoid various traditional fusion welding defects (such as air voids, joint tumours, fractures, and ejection) [13, 14]. When using the FSW technique to weld magnesium alloys, the induced heat would be substantially lower than the heat generated by the typical procedure of welding. Conditions after a joint are likely to end up with a big drop in deformation and residual stress [15].

The quality of weldments is determined by an intricate combination of process-based parameters (tool angle of tilt, tool speed, rate of plunge, tool traverse speed, vertical downwards force, tool pin design, etc.), material properties that are vital for the weldment (shear and yield stress, hardness, strength, etc.), and cooling technique [5, 16]. In FSW, materials to be welded (typically flat plates) must be rotated by the welding tool to achieve a precise strain of the plasticized material, and therefore, the generated torque at the junction between the work specimen and tool plays a vital role [10, 17]. As it lowers through the specimen for joining, the FSW tool often encounters *Y*-directional forces. When the tool pin moves in the direction of welding, it also feels a longitudinal force called the *X*-force. This force is mostly caused by the resistance of the plate's plasticized metal over the tool pin region [7, 13].

A considerable amount of *Y*-force is an unavoidable need for efficient welding because, at the trailing edge of the tool pin, heat production and plasticized metal combining are improvised. Aside from these factors, the shape of the tool is also very important. It affects how much heat is generated, how much the metal deforms when it is softened, and how the metal mixes at the weldment line where the plates meet, which in turn affects the quality of the joint [4, 18].

Yang et al. [18] examined the AA6061-T6 plates by FSW using seven tool pins with varied geometry. The shoulder shape of the tool and tool pin was found to have a vital part in heat generation, at the plunging phase the tool torque fluctuation as well the nugget zone area estimation. A tool that has fluted shoulders and corrugated pins produces grains that are highly refined in the weldment region, but pins with flat faces produce faulty junctions with nonhomogeneous shaped grains in their NZ. Kumar et al. [19]'s FSW was used to produce junctions of various aluminium alloys (Aluminium 6061 and Aluminium 5083) using tools with 3 independent pin geometries. It was found that joints made of different kinds of aluminium alloy with a tapered tool pin and threaded profiles were the strongest.

In major accordance with regard to tool pin shape impact on FSW [20–22], from the literature, it is clear that FSW is produced by changing the speed of the tool, and the tool tilt angle is either fixed or not considered. There are extremely less works of literature. References [23–25] have made reviews on the FSW regarding the effect of tool tilt angle. For instance, Zhai et al. [23] the outcome of angle of tilt on production of heat, metal flow behaviour, and field temperature during friction stir with regard to tool pin shape impact on FSW, it is clear from the literature that FSW is produced by changing the speed of the tool, and the tool tilt angle is either fixed or not considered [20–22]. There is extremely little literature that has reviewed the FSW regarding the effect of tool tilt angle [23–25]. For instance, Zhai et al. [23] the outcome of the angle of tilt on the production of heat, metal flow behaviour, and field temperature during friction stir welding was explored both experimentally and numerically. When compared to a 0° angle of tilt, a slanted angle of 2.5° provides a forceful forging effect at the trailing side, hence boosting the maximum temperature with the concomitant escalation in the plasticized metal flow [26]. The FSW of AZ31B and AZ91C magnesium alloys was tested, and the joints had a strength of 186 MPa, which is 78.81 percent higher than that of AZ91C and 70.72 percent higher than that of AZ31B, another parent metal. Intermetallic phased elements, like Mg₁₇Al₁₂, can be found in different places on fractured surfaces. These elements have made the nugget zone more fragile and decreased the joint's tensile strength.

The maximum tensile strength of the aluminium base metal, which was manufactured at a 20° tilt angle, was improved by 75% [27]. At the upper tilt angle, the increased heat production and axial force cause the separation of steel fragments on the aluminium matrix and the formation of the intermetallic complex Al-Fe. An investigation was conducted into the effects of FSW tool rotation speed (rpm), travelling speed (*V*), tilt angle (tilt), and plunge depth on material flow, joint tensile strength, flexural strength, impact energy, and hardness. The joint with the highest strength is achieved at 2200 rpm with a travelling speed of 105 mm/min at 2.5° tilt and a plunge depth of 1.2 mm [28]. The greatest values for tensile strength, flexural strength, and impact energy were 82% (about 55 MPa), 76% (about 61 MPa), and 75% (about 19 kJ/m², respectively). According to fractographic research, the surface has diverging lines that grow outside of the fracture start zone [29]. The effects of tilt angle, plunge depth, and tool offset were examined in the friction stir welding of poly (methyl methacrylate) *T*-joints. The greatest flexural and tensile strengths of friction stir welded joints were approximately 93% and 90% of as-received polyethylene at 0 mm offset, 2° tilt angle, and 0.2 mm plunge depth added (methyl methacrylate) [30].

It was tested on a different FSW polycarbonate (PC) sheet and an aluminium alloy AA5058 lap. The highest values of tensile and bending strengths were achieved at 68.2% (46 MPa) and 69.4% (60 MPa), respectively. Fractography showed that the AA5058 alloy/PC contact broke during the tensile test below and in the middle of the stir zone. In another investigation, the effects of submerged

temperatures (three levels of 273 K, 298 K, and 333 K) on the metallurgical and mechanical characteristics of the joints were analysed [31]. A lower hardness was attained in submerged welding. However, it can be boosted by processing it with warm water. The butt-joint of AA5083 Al-Mg alloy and A441 AISI steel sheet had been accomplished in ambient air without overcooling, and the examination was performed by immersing them in the cooling water medium at three different temperatures of 0°C, 25°C, and 50°C [32]. Based on the results of experiments, all of the samples fail at the joint interface along the IMC layer when the cooling medium is at room temperature and has the best tensile strength (310 MPa) and elongation (13%).

In a nut-shell, it can be ascertained that FSW with tool variation of dimension and angle of tilt work is limited, thereby examining the tool tilt effect, and the shape of the tool should be investigated critically. This work focuses on evaluating the angle of tilt and two unique tool pin shapes with and without threads.

2. Materials and Methods

The entire research project was carried out using friction stir welding equipment, which is a versatile semiautomated machine. AZ91B Mg alloy plates with rectangular dimensions of 110 × 50 × 6 mm were stacked in the specially designed fixture to achieve a butt type of junction throughout the operation. Table 1 lists the constituents of this AZ91B rectangular plate, as well as the appropriate weight percent and mechanical parameters.

The tools employed in this study were made of high-speed steel M42 grade that had been 63HRC hardened. In this research, tools with 2 different tool pin shapes are used, which are cylindrically tapered pins with threads (TPNT) and without threads. Figure 1 shows a view of the two unique tools being used.

As shown in Figure 1, all of the tools used in this work have the identical tool dimensions, which include a taller and bigger external shoulder (2 cm in diameter and 5 cm in length), trailed by a smaller length of tool and shoulder diameter (1.5 cm in all dimensions). With the help of a single-factor experimental design [27], the main goal of the research is to look at how the angle of tilt affects the production of different torques and forces by two different-shaped tools. Because of this, process variables like tool speed (1000 rpm) and tool traverse (1.5 mm/sec), which were found in the preexperimental work, were kept the same throughout the study.

The spindle torque, *Y*-force, and *X*-force are measured using a strain gauge-type load cell installed into the bottom of a specially designed clamp. Figure 2 depicts a pictorial representation of the work, along with the depiction of the *Y*-force and *X*-force directions, rectangular plates, the AZ91B control board, the friction stir welding machine, and the load cell. The load cell used is a semiautomated model, which has a fixture that is unique for maintaining plates together.

A dwell period of 3 seconds, a plunging rate of 25 mm/sec, and a plunge depth of 0.2 mm were all considered for

analysis. The majority of the experimental studies [33–36] show that defect-free friction stir welded connections were obtained when an angle of tilt of less than 3°–4° was used. At the same time, several researchers [37, 38] have shown that an angle of tilt of 0° is desirable for high-quality joints. Based on those previous works, the angles of tilt of 0°, 1°, and 2° were used in this study.

3. Results and Discussion

A set of tools, TPT and TPNT, were used to join AZ91B-Mg alloys together. In this section, the tool tilt effect, spindle torque vertical force acting downwards (*Y*-force), and force met by the tool pin axially (*X*-force) are analysed with macrostructural characteristics of welded specimens being investigated, followed by microstructural analysis through SEM images. Tensile characteristics were evaluated and compared with the parent alloy material of the specimens.

Figure 3 illustrates the torque deviation induced in the spindle torque vertical force acting downwards (*Y*-force) and the force met by the tool pin axially (*X*-force) with regard to the used tool tilt angle. Once the transverse initiates after the dwell completion, the force and torque numerical mean values are considered for the analysis. The beginning of the transition phase (moment at unstable forces and torque) had also been taken into interpretation with the average value, since the difference between them is not very big, and the overall drift of friction stir weldments is to all mean values.

The weldment made with various tool pin shapes with its grain size in the nugget region is briefed in Table 2. The nominal diameter of the grain size is calculated by the mean linear intercept approach. From this table, it is clear that as the tool pin angle rises, there is a proportionate grain size increase at the nugget zone. Joints made with TPT have smaller and finer grain sizes when compared to joints made with tapered pins without threads. The weldment made from a tapered tool pin with a threaded shape at 0° produced more refined and smaller grains at the nugget zone, whereas the AZ91B weldment fabricated at 2° of tilt using the TPNT tool produced a bigger grain structure at the nugget zone.

EDX analysis of the weldments TPT tool at 0, 1, and 2 degrees of tilt reveals a large peak of oxygen (O), as well as miniature apexes of carbon (C), zinc (Zn), and a massive apex of magnesium (Mg) and aluminium (Al). These samples contained silicon (Si) particles as small as a few micrometres in size. A frequent scenario for AZ91B is the occurrence of higher percentages of aluminium (Al) and lower percentages of zinc (Zn). Al and Mg are important alloying ingredients for improving weldment characteristics [12, 19]. In this study, detailed research on the creation of specific strength-increasing components was not done because the main goal of the EDX as well as SEM tests was to confirm the occurrence of materials within the nugget region caused by different angles of tilt.

Tensile fractography was used in this research to examine the mechanism of fracture in which the constructed joints collapsed. Table 3 shows that the joints produced with the TPT tool at 0° and 2° degrees of tilt and the joints manufactured with the TPNT tool at 0° degrees of tilt had

TABLE 1: AZ91B properties and compositions.

| Name of the alloy | Al | Zn | Ni | Cu | Mn | Si | Fe | Mg | Tensile value | Yield value | % of extension |
|-------------------|-----|------|-------|------|------|------|-------|---------|---------------|-------------|----------------|
| AZ91B | 3.1 | 0.85 | 0.005 | 0.05 | 0.31 | 0.08 | 0.005 | Balance | 263 (MPa) | 178 (MPa) | 11.7 |

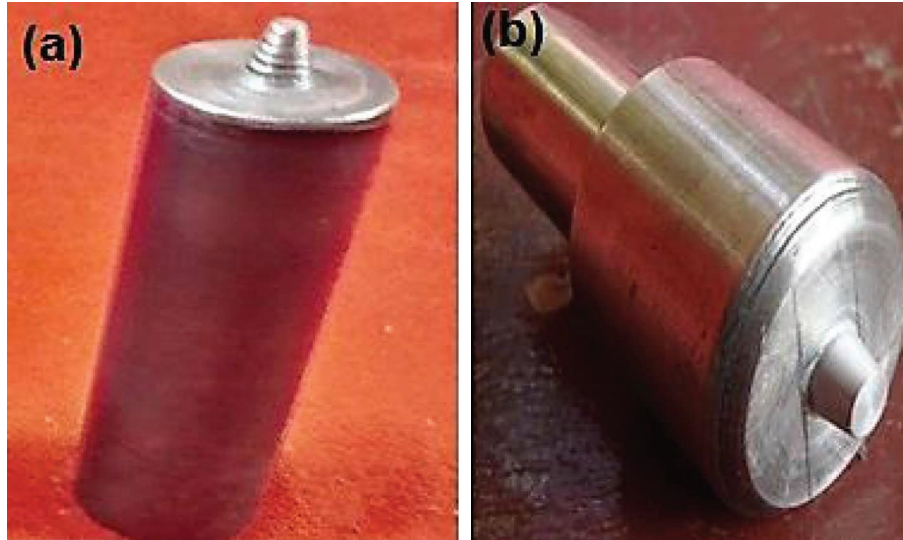


FIGURE 1: Picture of tool pins. (a) Tapered tool pin cylindrical shape with threads (TPT). (b) Tapered tool pin cylindrical shape without threads (TPNT).

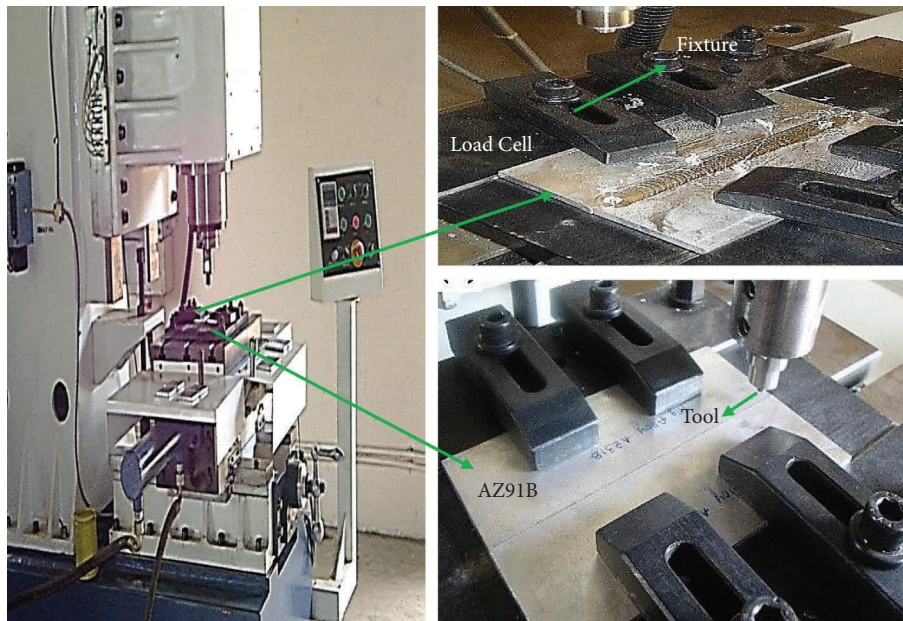


FIGURE 2: Research work setup.

dent-like variations in shapes, i.e., gaps that are visible at broad tear rims, suggesting that the specimen has undergone a fracture in ductile mode. Similarly, the cracked top layer or surface of weldments manufactured at 1° and 2° with the TPNT tool reveals the occurrence of dimple kinds of abysses or voids and flat surfaces, which are featured in the fracture

type and the trans-granular type. Simultaneously, joint surfaces produced from the fracture specimen with 1° of tilt with the TPT tool show the existence of many layered surfaces and platforms. The brittle type of the fracture causes the broken surfaces of the joints mentioned above to have these unique features.

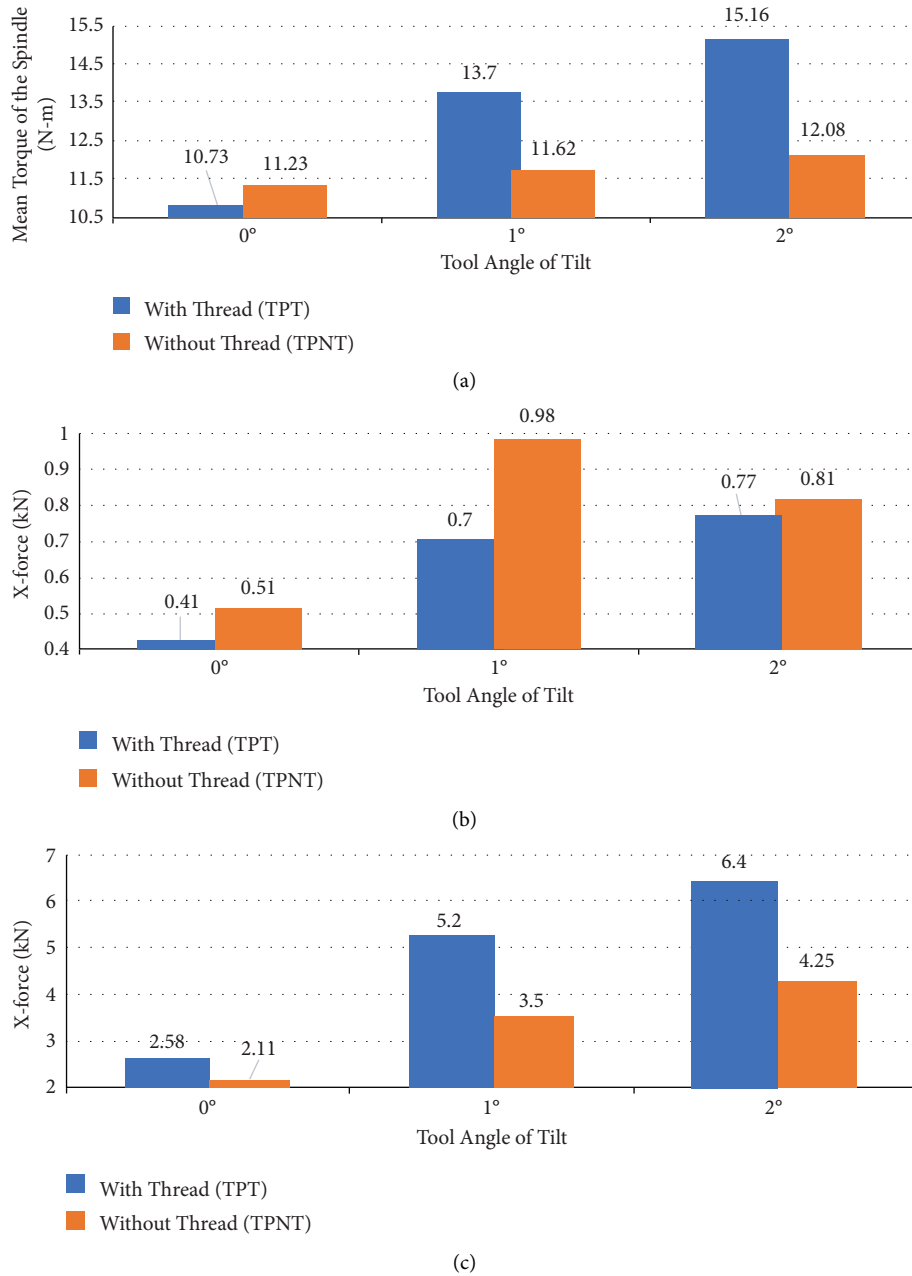


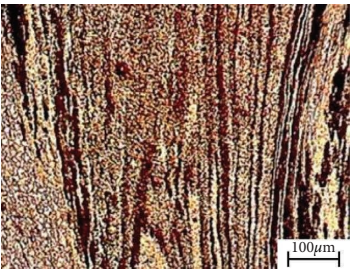
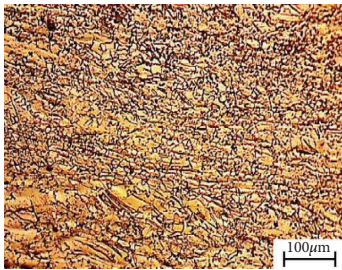
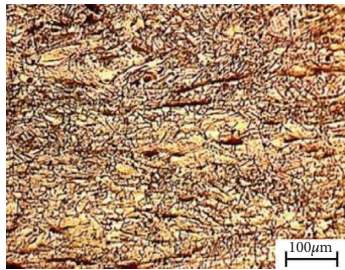
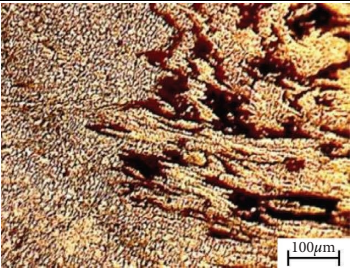
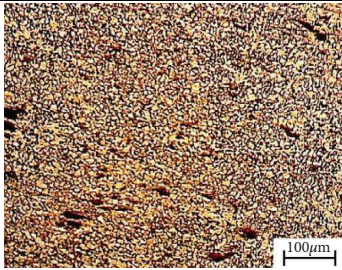
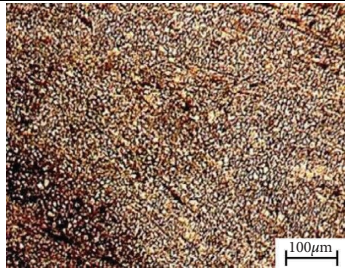
FIGURE 3: (a) Torque induced in the spindle, (b) longitudinal force (X-force) in tool pin, and (c) (Y-force) acting vertically downwards in reference to the angle of tool tilt.

3.1. Force and Torque Generation. Once the transverse initiates after the dwell completion, the force and torque numerical mean values are considered for the analysis. The onset of the transition phase, when forces and torque were unstable, was also considered with a mean value since their connected disparity is insignificant, and the overall drift of friction stir weldments to all mean values. From Figure 2, it can be seen that when using a 0° angle of tilt, both the TPT and TPNT tools are induced to a smooth Y-force, which is in the vertical direction with a spindle torque too. Similarly, with 1° and 2° of tilt, the two tool pin designs experienced an increase in spindle torque and Y-force during the early conversion phase. The primary cause of such behaviour can

be linked to the requirement for a massive amount of torque, and the force at the primal phase is for more metal plasticization, but the upsurge in tilt of tool at the shoulder region at weldment heat is not generated at the required quantity [20, 39].

Moreover, as the degree of tilt increases, so does the amount of metal to be moved. However, the thermal salving of the material achieved has been insufficient for that large amount of metal compared to other welding methods. It circuitously adds to X-force abnormalities. The changes related to torque as well as forces appear to hurt the tool’s ability to last. Since the TPT tool achieved more torque and Y-force than the TPNT tool, the TPT tool had a lower mean value of X-force for all of the utilized

TABLE 2: Grain size in the nugget zone.

| Shape of tool | 0° angle | 1° angle | 2° angle |
|-------------------|---|--|---|
| TPNT |  |  |  |
| Size of the grain | 13.1 µm | 15.7 µm | 13.9 µm |
| TPT |  |  |  |
| Size of the grain | 10.2 µm | 12.1 µm | 13.2 µm |

degrees of tilt. This, in turn, causes additional heat to be generated, resulting in greater metal plasticization. Moreover, the plasticized metal flow is improvised by the support of threads in the profile of the TPT tool, reducing the force, i.e., X -force stressing the tool pin. In the usage of TPNT at 2° angle of tool tilt, a small decrease in X -force is noticed, but the value of X -force gets an increase in its value when working with a TPT tool from 0° to 1° angle of tilt. It clarifies the process where there is a considerable improvement in thermal plasticization, and the related metal flow has been reached at a specific degree of tilt, which is the threshold value above which the torque and Y -force get a high value, leading to a high value of frictional heat generation in the weldment [15, 23]. For the same reason, inconsistencies have been reduced at a higher tilt of the tool in TPT tools, despite the tool pin having a greater amount of softened material.

Due to the presence of the threads within the tool pin design, i.e., TPT tool, it precisely clobbers the plasticized metal flow, which ensures the proper movement of the material flow. Contrarily, the typical TPNT tool without the threads supports the greater quantity of plasticized metal flow. At higher tilt angles, the threaded tool properly maintains the plasticized metal flow by generating more heat through friction, which proportionally increases the thermal plasticizing effect of the weldment specimen, thereby improving the flow of metal flow is actuated by the tool pin with threads. But as the tool tilt angle gets bigger, the frictional heat generated by the TPNT tool isn't in the right range or isn't enough. This causes the weldment to have uneven spots or holes. This is the reason behind the variation in x -force at the higher tilt of the TPNT tool, and fluctuations are noted in the x -force for the prolonged feasibility of tool shape and metal flow [40]. The larger discrepancies, nonconformities, and irregularities of the material flow around the pin as well as the higher variations in the stress are put on the pin when the tool moves.

3.2. Microstructure and Macrostructure. Table 4 illustrates the cross-sectional macrostructure in joints manufactured using tools with tapered pins with threads (TPT) tool and without threads (TPNT) tool. Except for the zone of agitation of the joint manufactured at 0° angle of tilt, the rest of the 2 weldments made using the TPNT tool don't show onion ring characteristics. At the very instant, this onion kind of circle had been seen very commonly within the tool stir region produced by the TPNT tool [41]. The onion ring shape comes from the way through the softened metal flow. From Table 4, it may be deduced that the TPNT tool with a 0° angle of tilt has onion ring-type characteristics in its nugget zone. At the same time, when the degree of tilt increases, the presence of these onion ring-type characteristics within the nugget regions of the joints manufactured through the TPNT becomes less noticeable. In the FSW process, the metal is driven out by the tool shoulder by its motion from the side of initiation to the descending side. The metal is then squeezed using the pin of the tool and driven across the surfaces of the tool pin from the side of descendance to initiation. A portion of the ejected metal migrates beneath the pin and to the side of progress. The utilized tool's shoulder on the progression sideways likewise forces the softened material downhill via the progression region of the tool [27].

The interactions between the two metal flows in the progression region (a downward flow of weldment metal caused by the shoulder region and a metal flow from the rebuttal area to the tool pin surface area) have led to this onion-ring-shaped pattern at the nugget region [11, 25]. When using the TPNT tool at a 0° angle of tilt, the generated X -force is more consistent than at other degrees of tilt. Similarly, at a 0° angle of tilt, the Y -force parameter value is less. As a consequence, at a 0° angle of tilt, the tool shoulder and pin created the plasticized metal flow and prevented

TABLE 3: SEM images of fractured zone.

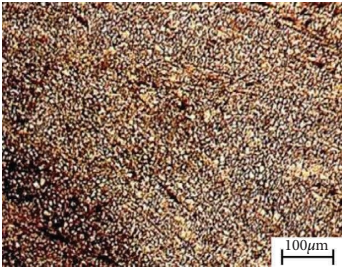

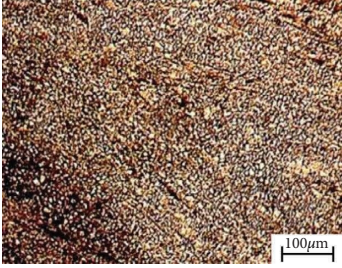

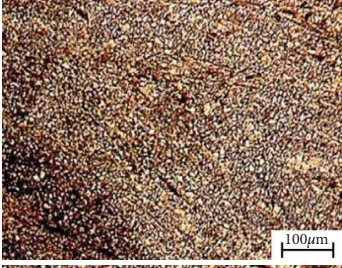
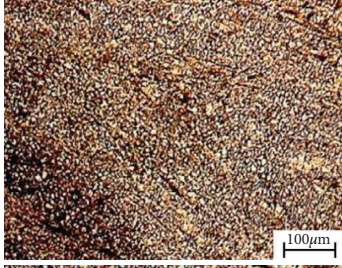
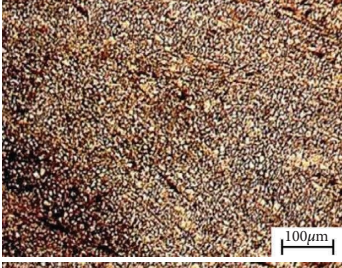

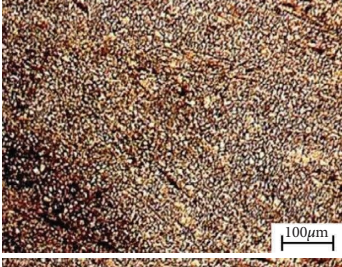

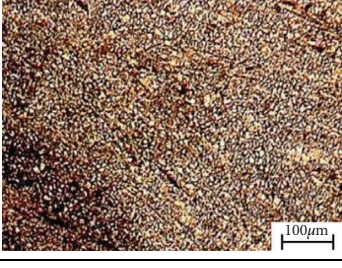
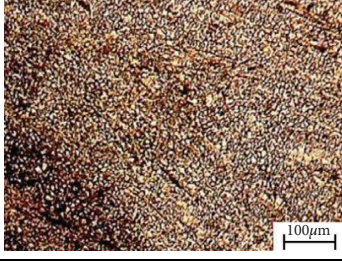
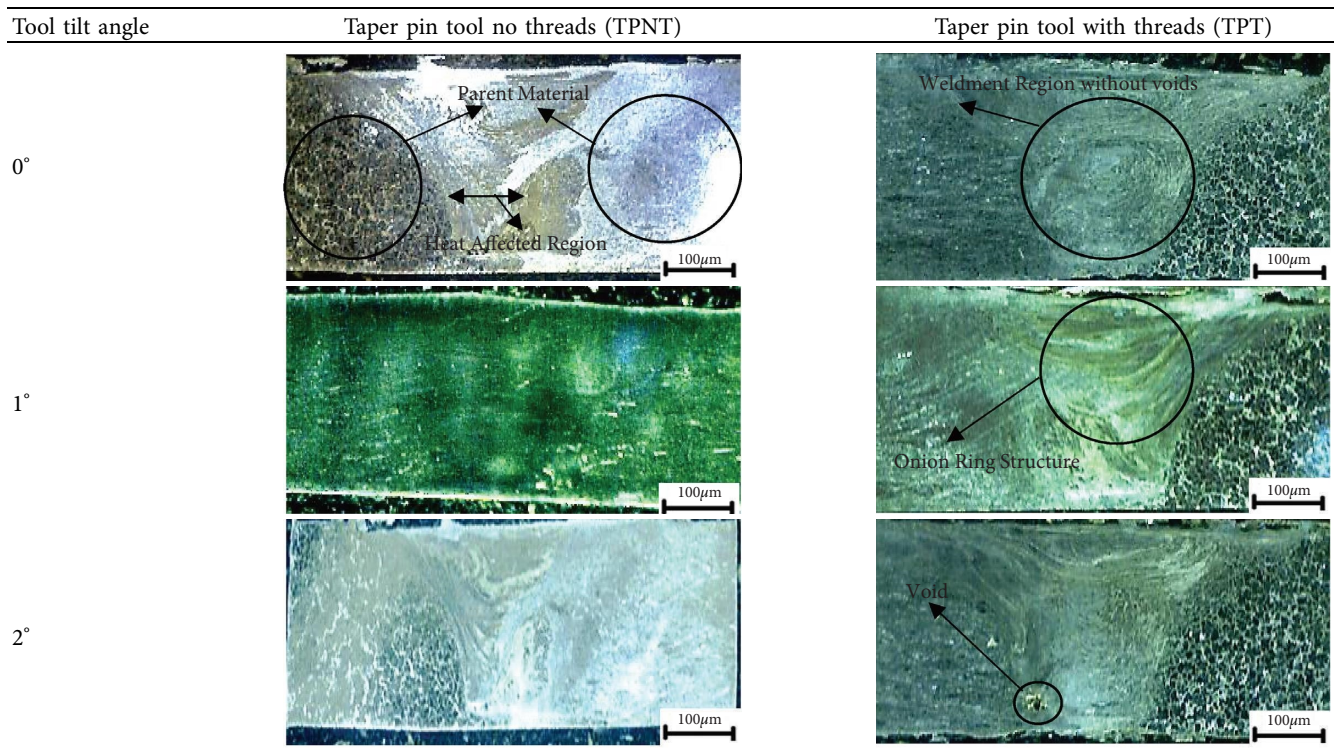
| Tool type and tool tilt angle | Fractured surface picture | Fractures area SEM pics |
|----------------------------------|---|---|
| TPNT tool and 0° tool tilt angle |  |  |
| TPNT tool and 1° tool tilt angle |  |  |
| TPNT tool and 2° tool tilt angle |  |  |
| TPT tool 0° tool tilt angle |  |  |
| TPT tool 1° tool tilt angle |  |  |
| TPT tool 2° tool tilt angle |  |  |

TABLE 4: Macrostructural cross-sectional views.



severe contact of these flows of metal, resulting in onion ring-type features. At 0° and 2° of tilt, the pin's flow of plasticized metal is less stable because the X -force changes are getting bigger.

The Y -force has surpassed the X -force in dominance and is continuously expanding. Because the tool pin and shoulder interacted, the metal flowed in a way that caused a deviation in the pin-generated plasticized metal flow [24]. This meant that onion ring-like features didn't form in the nugget zone. A distinct zone of the nugget may be observed by increasing the angle of tilt from 0° to 1°. Because the resulting forces were insufficient to breakdown the oxide layer on the neighbouring sides of the surface of the AZ91B base plate, a kissing bond formed. Similarly, the downward movement of the plasticized metal was insufficient and subsided root gap formation. But when the angle of tilt is changed from 1° to 2°, it can be noted that in the nugget region, the root gaps are removed. The onion circles could be seen in the nugget zone of all manufactured joints with the TPT tool as well. It is clear in all tool tilt angles that the plasticized metal flow was proper and steady due to the presence of the threaded structure. The TPT tool's onion ring characteristics show an amorphous layer.

The onion ring's inclined characteristics are not immaculate and have been separated into many distinctive layers [7, 13]. In the bottom section of such onion circles, it could be observable that all of the joints are constructed at three unique degrees of tilt, i.e., 0°, 1°, and 2°. However, the top portion of the onion circles has been poorly perceptible in joints at 0° as well as 1° of tool angle. The phenomenon demonstrates that there is 0° to 1° of tilt. The plasticized metal

flow was protruding in the upper region of the nugget zone, which disordered the flow of the metal in between the layers of the metal which is guided by the tool shoulder. In a 2° angle of tilt, such an onion circle structure had been visualized in the upper region of the nugget zone. That proves that when the angle of tool tilt increases the shoulder-driven and pin-driven metal flow, a balance is attained. The variability in the X -force is modest in these joints manufactured at 2° of tilt, suggesting a significantly more continuous plasticized metal flow generated by the welding tool pin. In comparison with the other degrees of tilt, the 2° angle of tilt X -force mean value is higher, which indicates the tool pin is more effective in pushing the plasticized metal [33, 42].

The other deduction is that when the angle of tilt increases from 0° to 1°, the breadth of the nugget zone expands, regardless of the shape of the tool pin used. However, increasing the angle of tilt from 1° to 2° results in a lessening in the breadth of the nugget area for both pin designs. Because of the increased Y -force as well as spindle torque at greater degrees of tilt, a greater input of heat was obtained, resulting in the salving of the material [28]. It might have happened as a result of an increase in sliding contact between the base plate and the instrument in use. Moreover, with an increase in the angle of tilt, the plasticized flow of metal increases in the downward direction. This caused lessening of the metal deformation at the nugget zone in direction parallel to the cross of the weldment joint cross-section proportionally reducing the width of the nugget zone formed by 2° angle of tilt. The formation of an equal-sized and uniform grain structure

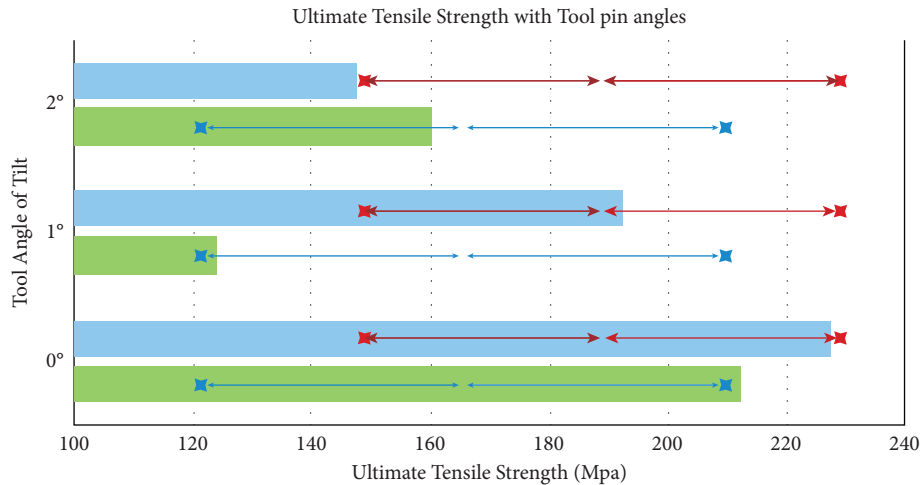


FIGURE 4: Comparison of ultimate tensile strength with tool pin angles.

in the nugget zone is due to dynamic recrystallization [38].

With an upsurge in the used tool tilt, the size of the grains may be observed to increase concurrently from Table 2. When the joints manufactured with the TPT tool were compared to the tools fabricated with the TPNT tool, fine-sized grains were discovered. This demonstrates that the tool pin's threads had a vital role to play in improving the plasticized metal flow [43]. The Y -force and spindle torque values continue to increase with the tool tilt angle.

The generation of frictional heat increases, reaching a peak temperature and a longer cooling period due to the increase in Y -force as well as torque parameters [20, 23]. As a result, the duration of exposure to the heat in the nugget region has increased. Under these favourable circumstances, alloys of magnesium are normally more responsive to grain development, which has led to the rise in grain size with regard to tool tilt [13, 40].

3.3. SEM and EDAX. The SEM images taken at the area of the boundary between the original alloy and nugget zone, the thermo-mechanically transmuted area, and the zone of nugget in joints are detailed in Table 5. The presence of higher percentages of oxygen, aluminium, and other elements shows the presence of intermetallic components of Mg17Al12. The presence of substantial quantities of oxygen (O), aluminium (Al), and carbon (C) in these intermetallic elements was due to a phenomenon known as reaction-based diffusion that happens within the elements of oxygen and carbon existing within the parent metal (AZ91B) and utilized tool. Due to frictional heat generation, the base metal surface of the AZ91B alloy at the welding interface region is prone to high plastic deformation. Mg clings to the surface of the tool pin as a consequence of the bonding between the HSS tool surface and the plasticized magnesium alloy.

At higher temperatures, a reaction-based diffusion phenomenon occurs on the surface of a high-speed steel tool, generating Mg17Al12 brittle intermetallic components on

the tool pin's surface [15, 21]. These brittle intermetallic elements breakdown off the pin area and become coagulated within the nugget region during subsequent joining of the AZ91B plates at greater temperature and stress. There are brittle intermetallic mixtures in the nugget region, such as Mg17Al12, which is fabricated by the TPT tool at 0°, 1°, and 2° angles of tilt due to the great number of variations in X -force employed on the tool pin and the larger confrontation against the plasticized metal flow around the tool pin surface. Table 6 shows an EDX spectroscopy analysis of the FSW weldments, the effect of frictional heat produced by the tool, and different degrees of deformation caused by changes in the tool tilt and the tool shape profile, which can be used to understand microstructural characteristics.

In the same instant, welding joints fabricated by the TPNT tool pin at 0°, 1°, and 2° angles of tool tilt at the nugget zone of specimen traces of carbon and oxygen were not observed. An EDAX examination of the nugget zone of the welded joints reveals the presence of lower quantities of silicon, manganese, and other elements. They are the base metal alloying elements (AZ91B), and the presence of these components verifies the occurrence of intermetallic in the combination of materials Mg-Si-Mn at the weldment nugget zone [16, 35].

3.4. Tensile Fractography. The specimens of the welded joints were submitted to tensile testing to evaluate the influence of the tool pin shape, degree of tool tilt angle, and corresponding demonstrated values in tensile strength. From Figure 4, it is to be noted that joints normally, regardless of the degree of tool tilt used, weldments from the TPT tool display higher effectiveness in tensile characteristics than the ones produced with the TPNT tool. It is also worth noting that the TPT tool demonstrates a consistent and incessant decrease in tensile-related parameters while simultaneously increasing the angle of tilt. Such a characteristic is not visible in joints formed with the TPNT tool. Weldments from the TPT tool at an angle of tilt of 0° had the maximum value of tensile strength-related characteristics.

TABLE 5: SEM images.

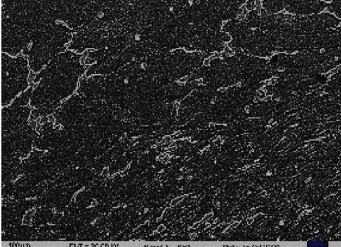
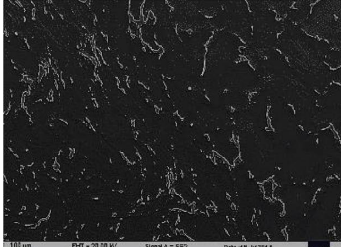
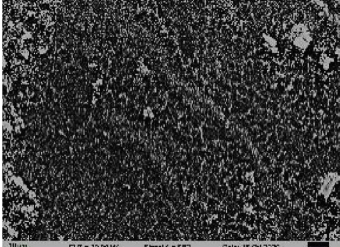

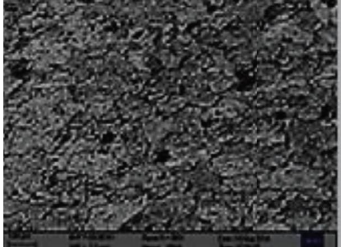
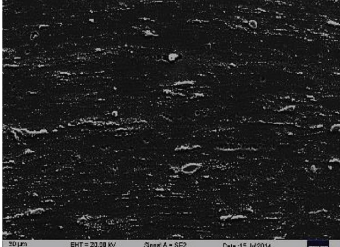
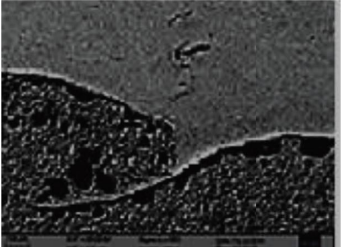
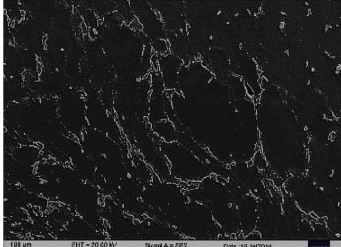
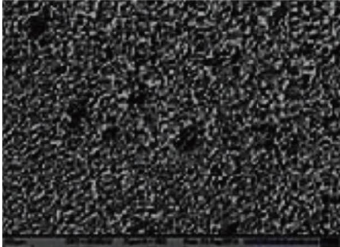
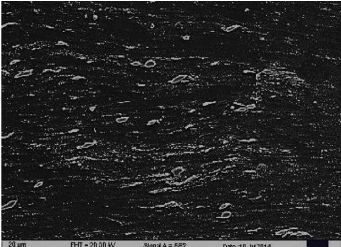
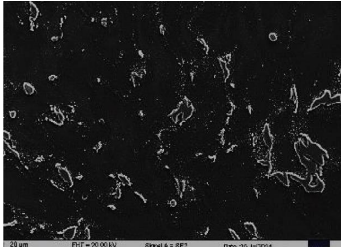
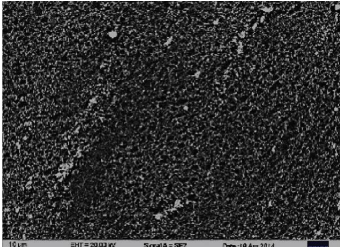
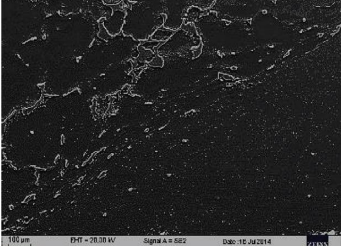
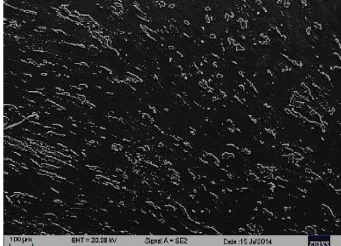

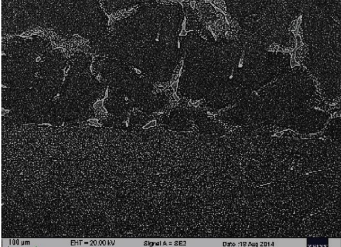
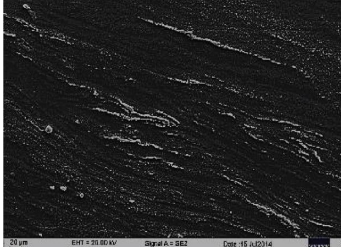


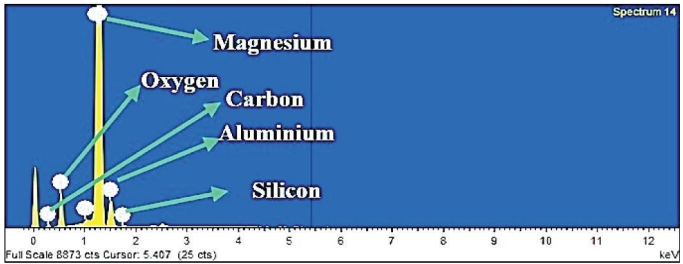
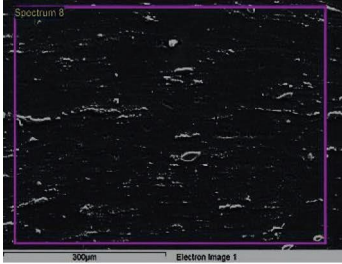
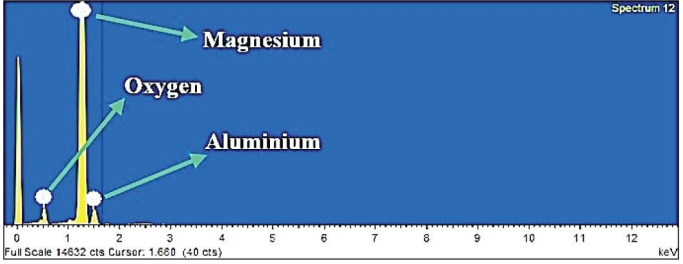
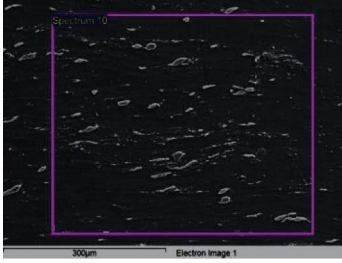
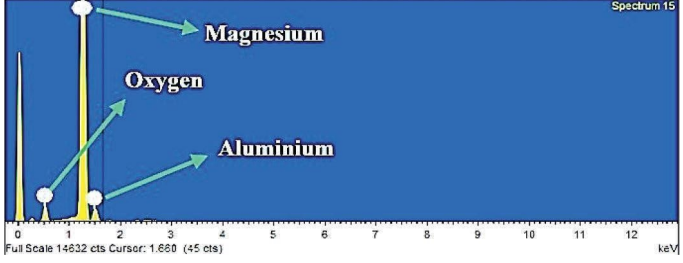
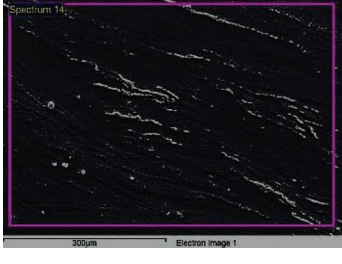
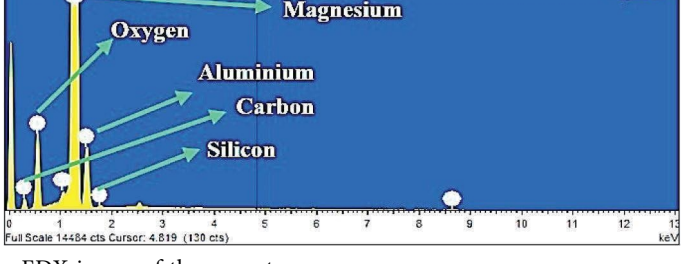
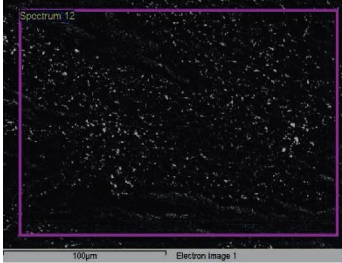
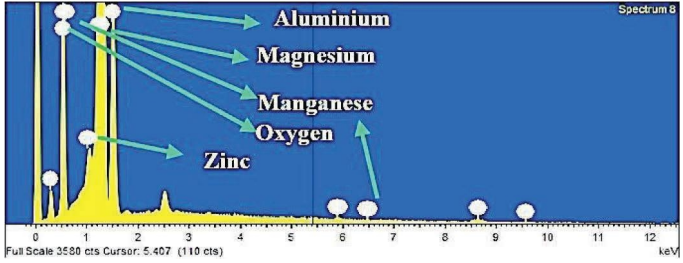
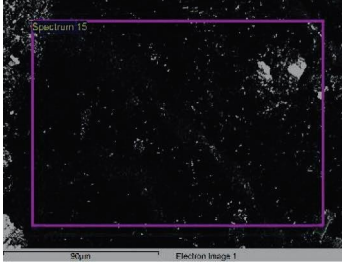
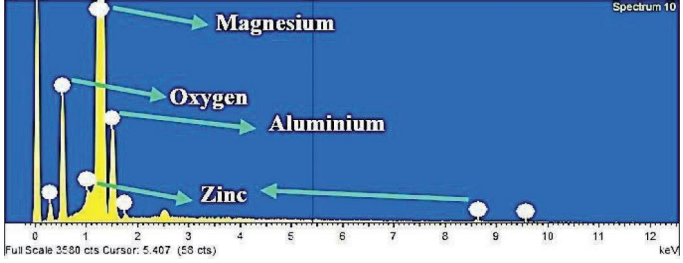
| Tool type and angle of tool tilt | Boundary region—nugget zone and parent material | Thermo-mechanically renovated region | Nugget zone |
|----------------------------------|---|--|---|
| TPNT tool and 0° tool tilt angle |  |  |  |
| TPNT tool and 1° tool tilt angle |  |  |  |
| TPNT tool and 2° tool tilt angle |  |  |  |
| TPT tool 0° tool tilt angle |  |  |  |
| TPT tool 1° tool tilt angle |  |  |  |
| TPT tool 2° tool tilt angle |  |  |  |

TABLE 6: EDX images.

| Tool type and angle of tool tilt | EDX image of the nugget zone | |
|----------------------------------|---|--|
| TPNT tool and 0° tool tilt angle |  |  |
| TPNT tool and 1° tool tilt angle |  |  |
| TPNT tool and 2° tool tilt angle |  |  |
| TPT tool 0° tool tilt angle |  |  |
| TPT tool 1° tool tilt angle |  |  |
| TPT tool 2° tool tilt angle |  |  |

At 2° of tilt, the joint made with the TPT tool has the least amount of tensile strength.

Inferring from Figure 4, the increase in the angle of tilt showed a decreasing trend in tensile strength for the TPT tool, with a maximum value of 232 MPa, and about 88.2% compared to the parent alloy material was exhibited by the weldment made with a 0° angle of tilt and the TPT tool. The grain size at the nugget region increased with respect to the angle of tilt generated by the TPT tool, as presented in Table 3. Moreover, for joints made with the TPNT tool, the differences in grain size in the nugget zone do not follow a consistent pattern in relation to the degree of tilt used. The grain size of the joint produced at 1° angle of tilt utilizing a TPNT tool is greater than the grain size created at 0° and 2° tool tilt angles. The least strength (124 MPa) from tensile tests is shown by the weldment specimen fabricated at 1° angle of tool tilt with TPNT tool pin of all the manufactured welding specimens because of the occurrence of large grains that are large at the nugget zone [22, 44]. The larger structure of the grains at the nugget zone in the weldment made with the TPNT tool at a 1° angle of tilt is quickly explained by the variation in the amount of frictional heat generated, the formation of secondary phase intermetallic constituents, and the flow of softened material, all of which are affected by the shape of the tool pin and its effect on the amount of plastic deformation [31].

Specimens retrieved from joints manufactured with the TPT tool at 1° and 2° degrees of tilt had fractures at their nuggets. The joint sample manufactured with the TPT tool at 0° angle of tilt, on the other hand, has fractured at its thermo-mechanical reformed area on the side of progression. Because the weldment is brittle, the stress intensity at the nugget zone is not linear. This causes the weldment to have low values during tensile testing, which causes the nugget zone to break at 1° and 2° of tilt of the TPT tool.

Specimens taken from joints constructed with the TPNT tool at 0° angle of tilt underwent fracture by ductile mode in their thermo-mechanical transformed zone. It is evident from Figure 4 that this joint has displayed a significant value in mechanical strength in comparison to two other joints constructed at 1° and 2° degrees of tilt (using the TPNT tool). Deep inspection of the cracked weldment made by tilting it at an angle of 1° (using the TPNT tool) shows that the tensile fracture followed a unique curved shape. Typically, this fracture or failure would have started at the zone of the nugget base as the zone had the minimum stirring effect by the tool and spread in the form of a kissing bond, making the failure rate high in testing for tensile strength [18, 36].

For the weldments manufactured with the TPT tool, a declining trend in tensile strength can be noted, along with an increase in the angle of tilt (as shown in Figure 4). Any macrostructural abnormalities were not found for the joints manufactured utilizing the TPT tool at 0° angle of tilt, and on the outside of the nugget zone, this type of weldment encountered failure (in the thermo-mechanically transformed zone on the advancing section). Tensile strength ratings for joints prepared at 1° of tilt (using the TPNT tool) and 2° of tilt (using the TPT tool) were the lowest of any produced joints. The existence of intermetallic elements that are stiff and tough in character was the primary cause of these low tensile

strength values [10, 25]. Table 6 also shows that most of the welded samples have cracks right away in the nugget zone, except for the sample of the weld made with a 0° angle of tool tilt and a TPT tool. This sample has a crack on the side where the thermomechanical transformation happened.

4. Conclusions

This research reveals the variation of the angle of tool tilt using two varied tool pin structures on varied friction stir weldments of AZ91B alloy, such as mechanical strength, spindle torque, forces encountered, and microstructural characteristics. The following are the inferences presented in this study endeavour.

- (i) At the interface of weldment between the AZ91B plates, spindle torque and forces of friction were produced, which increased with the increase in the angle of tilt. Regardless of the tool pin design used, a smooth distribution of spindle torque and FSW-associated forces was observed at a 0° angle of tilt. Because of the increased depth of dive at the trail's edge, *Y*-force increases with the angle of tilt. Because of the use of the TPT tool, the tool-workpiece area of contact has expanded, which induces high *Y*-force and spindle torque values irrespective of the degree of tilt.
- (ii) The TPT tool had an *X*-force value of less compared to the force value produced by the TPNT tool because the high torque and *Y*-forces produced by the TPT tool gave rise to the evolution of a high frictional heat, which promptly improved the plasticized flow of the metal, which decreased the forces resisting that are induced in the tool pin. These things have also indirectly helped to make the oscillations of the joining force less.
- (iii) Onion ring-like characteristics were noticed in weldments created with the TPT tool. Onion ring-type characteristics can't be easily viewed in joints created using the TPNT tool. The increased plasticized metal flow caused by the tool pin with threaded structure TPT has supported the formation of the onion ring shapes in the joint of the weldment. The thickness of the nugget zone of manufactured joints has decreased as the angle of tilt has gone up.
- (iv) The weldments made with the TPT tool showed an increasing trend in the grain size as the angle of tilt increased at the nugget region.

The tensile characteristics of joints manufactured with the TPT tool show a diminishing trend with an increase in the angle of tilt. The maximum tensile strength of 232 MPa, i.e., 88.2% of the parent material tensile strength value, was achieved by a 0° angle of tilt by the TPT tool.

Data Availability

The data used to support the findings of this study are included in the article.

Conflicts of Interest

The authors declare that there are no conflicts of interest regarding the publication of this paper.

References

- [1] D. Leśniak, A. Wassermann, M. Dziki, K. Zaborowski, and H. Jurczak, "Susceptibility for extrusion welding of AlMg alloys," *Archives of Civil and Mechanical Engineering*, vol. 19, no. 1, pp. 20–31, 2019.
- [2] R. Raj Mohan, R. Venkatraman, S. Raghuraman et al., "Processing of aluminium-silicon alloy with metal carbide as reinforcement through powder-based additive manufacturing: a critical study," *Scanning*, vol. 2022, Article ID 5610333, 14 pages, 2022.
- [3] Y. M. Baqer, S. Ramesh, F. Yusof, and S. M. Manladan, "Challenges and advances in laser welding of dissimilar light alloys: Al/Mg, Al/Ti, and Mg/Ti alloys," *International Journal of Advanced Manufacturing Technology*, vol. 95, no. 9-12, pp. 4353–4369, 2018.
- [4] S. Y. Ivanov, O. V. Panchenko, and V. G. Mikhailov, "Comparative analysis of non-uniformity of mechanical properties of welded joints of Al – Mg – Si alloys during friction stir welding and laser welding," *Metal Science and Heat Treatment*, vol. 60, no. 5-6, pp. 393–398, 2018.
- [5] U. K. Singh and A. K. Dubey, "Study of weld characteristics in friction stir welding of dissimilar Mg-Al-Zn magnesium alloys under varying welding conditions," *Journal of Materials Engineering and Performance*, vol. 30, no. 10, pp. 7690–7703, 2021.
- [6] S. P. Arunkumar, C. Prabha, R. Saminathan et al., "Taguchi optimization of metal inert gas (MIG) welding parameters to withstand high impact load for dissimilar weld joints," *Materials Today Proceedings*, vol. 56, pp. 1411–1417, 2022.
- [7] J. Liu, S. Niu, R. Ren, S. Ji, L. Wang, and Z. Lv, "Improving joint morphologies and tensile strength of Al/Mg dissimilar alloys friction stir lap welding by changing Zn interlayer thickness," *Acta Metallurgica Sinica*, vol. 32, no. 11, pp. 1385–1395, 2019.
- [8] M. R. Islam, M. Ishak, L. H. Shah, S. R. A. Idris, and C. Meric, "Dissimilar welding of A7075-T651 and AZ31B alloys by gas metal arc plug welding method," *International Journal of Advanced Manufacturing Technology*, vol. 88, no. 9-12, pp. 2773–2783, 2017.
- [9] X. Jiang and S. Chen, "Texture evolution and plastic deformation mechanism in magnetic pulse welding of dissimilar Al and Mg alloys," *Welding in the World*, vol. 62, no. 6, pp. 1159–1171, 2018.
- [10] P. Chai, W. Hu, S. Ji, X. Ai, Z. Lv, and Q. Song, "Refill friction stir spot welding dissimilar Al/Mg alloys," *Journal of Materials Engineering and Performance*, vol. 28, no. 10, pp. 6174–6181, 2019.
- [11] M. A. Mofid, A. Abdollah-Zadeh, F. M. Ghaini, and C. H. Gur, "Submerged friction-stir welding (SFSW) underwater and under liquid nitrogen: an improved method to join Al alloys to Mg alloys," *Metallurgical and Materials Transactions A*, vol. 43, no. 13, pp. 5106–5114, 2012.
- [12] R. Raj Mohan, R. Venkatraman, S. Raghuraman et al., "Influence of planetary ball mill parameters on powder flowability of AlSi10Mg with niobium carbide using central composite design (CCD)," *Advances in Materials Science and Engineering*, vol. 2022, Article ID 2869225, 11 pages, 2022.
- [13] J. Taendl and C. Poletti, "Influence of Al₃ (Sc, Zr) precipitates on deformability and friction stir welding behavior of Al-Mg-Sc-Zr alloys," *Berg Huettenmaenn Monatsh*, vol. 161, no. 7, pp. 330–333, 2016.
- [14] M. M. Husain, R. Sarkar, T. K. Pal, N. Prabhu, and M. Ghosh, "Friction stir welding of steel: heat input, microstructure, and mechanical property Co-relation," *Journal of Materials Engineering and Performance*, vol. 24, no. 9, pp. 3673–3683, 2015.
- [15] M. M. Swamy, S. Muthukumar, and K. Kiran, "A Study on Friction Stir Multi Spot Welding Techniques to Join Commercial Pure Aluminum and Mild Steel Sheets," *Transactions of the Indian Institute of Metals*, vol. 70, pp. 1221–1232, 2017.
- [16] D. Sunilkumar, J. Mathew, and S. Muthukumar, "Friction Stir Welding of 2.25Cr–1Mo Steel to AISI 316LN Stainless Steel," *Transactions of the Indian Institute of Metals*, vol. 73, pp. 1689–1693, 2020.
- [17] T. Wang, S. Shukla, S. S. Nene, M. Frank, R. W. Wheeler, and R. S. Mishra, "Towards obtaining sound butt joint between metallurgically immiscible pure Cu and stainless steel through friction stir welding," *Metallurgical and Materials Transactions A*, vol. 49, no. 7, pp. 2578–2582, 2018.
- [18] M. Yang, R. j Bao, X. z Liu, and C. q Song, "Thermo-mechanical interaction between aluminum alloy and tools with different profiles during friction stir welding," *Transactions of Nonferrous Metals Society of China*, vol. 29, no. 3, pp. 495–506, 2019.
- [19] P. S. Kumar and M. S. Chander, "Effect of tool pin geometry on FSW dissimilar aluminum alloys - (AA5083 & AA6061)," *Materials Today Proceedings*, vol. 39, no. 1, pp. 472–477, 2021.
- [20] S. D. D. Babu, P. Sevel, and R. S. Kumar, "Simulation of heat transfer and analysis of impact of tool pin geometry and tool speed during friction stir welding of AZ80A Mg alloy plates," *Journal of Mechanical Science and Technology*, vol. 34, no. 10, pp. 4239–4250, 2020.
- [21] H. J. Zhang, M. Wang, Z. Zhu, X. Zhang, T. Yu, and Z. Q. Wu, "Impact of shoulder concavity on non-tool-tilt friction stir welding of 5052 aluminum alloy," *International Journal of Advanced Manufacturing Technology*, vol. 96, no. 1-4, pp. 1497–1506, 2018.
- [22] A. Tiwari, P. Singh, P. Pankaj, P. Biswas, S. D. Kore, and S. Pal, "Effect of tool offset and rotational speed in dissimilar friction stir welding of AISI 304 stainless steel and mild steel," *Journal of Materials Engineering and Performance*, vol. 28, no. 10, pp. 6365–6379, 2019.
- [23] M. Zhai, C. S. Wu, and H. Su, "Influence of tool tilt angle on heat transfer and material flow in friction stir welding," *Journal of Manufacturing Processes*, vol. 59, pp. 98–112, 2020.
- [24] B. Singh, K. K. Saxena, P. Singhal, and T. C. Joshi, "Role of various tool pin profiles in friction stir welding of AA2024 alloys," *Journal of Materials Engineering and Performance*, vol. 30, no. 11, pp. 8606–8615, 2021.
- [25] M. Grätzel, A. Regensburg, M. Hasieber, J. A. Gerken, R. Schurer, and J. P. Bergmann, "Scaling effects during friction stir welding of aluminum alloys with reduced tool aspect ratios," *Welding in the World*, vol. 63, no. 2, pp. 337–347, 2019.
- [26] S. Yaknesh, K. Sampathkumar, and P. Sevel, "Effect of tool pin geometry and process parameters during FSW of dissimilar alloys of Mg," *Materials Research*, vol. 25, 2022.
- [27] M. Elyasi, H. Aghajani Derazkola, and M. Hosseinzadeh, "Investigations of tool tilt angle on properties friction stir welding of A441 AISI to AA1100 aluminium," *Proceedings of the Institution of Mechanical Engineers - Part B: Journal of Engineering Manufacture*, vol. 230, no. 7, pp. 1234–1241, 2016.

- [28] H. Aghajani Derazkola, A. Simchi, and F. Lambiase, "Friction stir welding of polycarbonate lap joints: relationship between processing parameters and mechanical properties," *Polymer Testing*, vol. 79, Article ID 105999, 2019.
- [29] A. Eyvazian, A. M. Hamouda, H. Aghajani Derazkola, and M. Elyasi, "Study on the effects of tool tilt angle, offset and plunge depth on friction stir welding of poly(methyl methacrylate) T-joint," *Proceedings of the Institution of Mechanical Engineers - Part B: Journal of Engineering Manufacture*, vol. 234, no. 4, pp. 773–787, 2019.
- [30] H. A. Derazkola and M. Elyasi, "The influence of process parameters in friction stir welding of Al-Mg alloy and polycarbonate," *Journal of Manufacturing Processes*, vol. 35, pp. 88–98, 2018.
- [31] H. Aghajani Derazkola, A. Eyvazian, and A. Simchi, "Submerged friction stir welding of dissimilar joints between an Al-Mg alloy and low carbon steel: thermo-mechanical modeling, microstructural features, and mechanical properties," *Journal of Manufacturing Processes*, vol. 50, pp. 68–79, 2020.
- [32] H. A. Derazkola and F. Khodabakhshi, "Underwater submerged dissimilar friction-stir welding of AA5083 aluminum alloy and A441 AISI steel," *International Journal of Advanced Manufacturing Technology*, vol. 102, no. 9–12, pp. 4383–4395, 2019.
- [33] R. K. Nath, P. Maji, and J. D. Barma, "Development of a self-heated friction stir welding tool for welding of polypropylene sheets," *Journal of the Brazilian Society of Mechanical Sciences and Engineering*, vol. 41, no. 12, p. 553, 2019.
- [34] H. F. Wang, J. L. Wang, DW. Zuo, and W. W. Song, "Application of stir tool force measuring dynamometer for friction stir welding of aluminum alloys," *Strength of Materials*, vol. 49, no. 1, pp. 162–170, 2017.
- [35] S. Memon, A. Murillo-Marrodán, H. M. Lankarani, and H. Aghajani Derazkola, "Analysis of friction stir welding tool offset on the bonding and properties of Al-Mg-Si alloy T-joints," *Materials*, vol. 14, no. 13, p. 3604, 2021.
- [36] S. Ji, Z. Li, Z. Zhou, and B. Wu, "Effect of thread and rotating speed on material flow behavior and mechanical properties of friction stir lap welding joints," *Journal of Materials Engineering and Performance*, vol. 26, no. 10, pp. 5085–5096, 2017.
- [37] L. H. Shah, A. Fleury, L. St-George, S. Walbridge, and A. P. Gerlich, "Evolution of process parameters in friction stir welding of AA6061 aluminum alloy by varying tool eccentricity," *International Journal of Advanced Manufacturing Technology*, vol. 109, no. 5-6, pp. 1601–1612, 2020.
- [38] P. Pankaj, A. Tiwari, P. Biswas, A. Gourav Rao, and S. Pal, "A three-dimensional heat transfer modelling and experimental study on friction stir welding of dissimilar steels," *Journal of the Brazilian Society of Mechanical Sciences and Engineering*, vol. 42, no. 9, p. 467, 2020.
- [39] G. Buffa, G. Ingarao, D. Campanella, R. Di Lorenzo, F. Micari, and L. Fratini, "An insight into the electrical energy demand of friction stir welding processes: the role of process parameters, material and machine tool architecture," *International Journal of Advanced Manufacturing Technology*, vol. 100, no. 9-12, pp. 3013–3024, 2019.
- [40] A. H. Baghdadi, Z. Sajuri, N. F. M. Selamat, M. Z. Omar, Y. Miyashita, and A. H. Kokabi, "Effect of intermetallic compounds on the fracture behavior of dissimilar friction stir welding joints of Mg and Al alloys," *International Journal of Minerals, Metallurgy and Materials*, vol. 26, no. 10, pp. 1285–1298, 2019.
- [41] S. Yaknesh, K. Sampathkumar, P. Sevel, and I. John Solomon, "Generation of force and torque during joining of AZ91C plates by FSW under distinctive tool tilt angle and their impact on mechanical strength and micro-structure," *Journal of Adhesion Science and Technology*, pp. 1–20, 2022.
- [42] Y. P. Zhao, L. F. Chen, S. J. Zhu, Yf Sun, and Sk Guan, "Clarifying effect of welding conditions on microstructure and mechanical properties of friction stir spot-welded DH590 automotive high-strength steel plates," *Journal of Iron and Steel Research International*, vol. 28, no. 2, pp. 232–243, 2021.
- [43] S. Memon, D. Fydrych, A. C. Fernandez, H. A. Derazkola, and H. A. Derazkola, "Effects of FSW tool plunge depth on properties of an Al-Mg-Si alloy T-joint: thermomechanical modeling and experimental evaluation," *Materials*, vol. 14, no. 16, p. 4754, 2021.
- [44] Z. Iqbal, A. Bazoune, F. Al-Badour, A. Shuaib, and N. Merah, "Effect of tool rotational speed on friction stir welding of ASTM a516-70 steel using W-25%Re alloy tool," *Arabian Journal for Science and Engineering*, vol. 44, no. 2, pp. 1233–1242, 2019.